Environmental evidence for net methane production and oxidation in putative ANaerobic MEthanotrophic (ANME) archaea

Karen G. Lloyd,[1,2]***** **Marc J. Alperin**[2] **and**
Andreas Teske[2]

[1]*Center for Geomicrobiology, Ny Munkegade 114, Bldg 1540, Aarhus University, 8000-Aarhus C, Denmark.*
[2]*Department of Marine Sciences, CB#3300, University of North Carolina at Chapel Hill, Chapel Hill, NC 27599, USA.*

Summary

Uncultured ANaerobic MEthanotrophic (ANME) archaea are often assumed to be obligate methanotrophs that are incapable of net methanogenesis, and are therefore used as proxies for anaerobic methane oxidation in many environments in spite of uncertainty regarding their metabolic capabilities. Anaerobic methane oxidation regulates methane emissions in marine sediments and appears to occur through a reversal of a methane-producing metabolism. We tested the assumption that ANME are obligate methanotrophs by detecting and quantifying gene transcription of ANME-1 across zones of methane oxidation versus methane production in sediments from the White Oak River estuary, North Carolina. ANME-1 consistently transcribe 16S rRNA and mRNA of methyl coenzyme M reductase (*mcrA*), the key gene for methanogenesis, up to 45 cm into methanogenic sediments. CARD-FISH shows that ANME-1 exist as single rod-shaped cells or pairs of cells. Integrating normalized depth distributions of 16S rDNA and rRNA (measured with qPCR and RT-qPCR respectively) shows that 26–77% of the rDNA (a proxy for ANME-1 cell numbers), and 18–76% of the rRNA (a proxy for ANME-1 activity) occurs within methane-producing sediments. These results, along with a re-assessment of the published literature, change the perspective to ANME-1 as methanogens that are also capable of methane oxidation.

Introduction

Anoxic coastal sediments produce large amounts of the greenhouse gas methane, but biological anaerobic methane oxidation consumes most of the upward diffusing methane before it reaches the overlying water (Reeburgh, 2007). This process is generally attributed to groups of methanogen-like archaea that have never been obtained in pure culture, but have been identified by molecular phylogeny and collectively named 'ANME' (for ANaerobic MEthanotroph) with suffixes 1, 2 and 3 (Hinrichs *et al.*, 1999; Knittel and Boetius, 2009). It is widely assumed that ANME archaea are incapable of obtaining energy from the net production of methane (Parkes *et al.*, 2007; Knittel and Boetius, 2009). Hence, the presence of ANME DNA sequences has been assumed to indicate anaerobic methane oxidation in a wide variety of environments including the oxycline of seawater, freshwater lakes, brine lakes, terrestrial aquifers, terrestrial mud volcanoes, microbial mats, hydrothermal vents, ancient marine sediments, petroleum-contaminated sediments, methane-producing marine sediments and oceanic hydrocarbon seeps (Knittel and Boetius, 2009).

The possibility that ANME archaea may be able to function as normal methanogens has not been adequately addressed. When Hinrichs and colleagues (1999) first coined the term 'ANME' to describe the archaea in methane seep sediments from Eel River Basin, they recognized that these organisms could be obligate or 'dominant' methanotrophs, normally functioning methanogens or methanogens operating in reverse. The possibility that ANME archaea could be methanogens operating in reverse was dismissed on three grounds: (i) ANME archaea had never been detected in methanogenic sediments, (ii) ANME-1 would represent a new order of methanogens and (iii) a metabolic pathway for reverse methanogenesis was unknown. Several plausible pathways for reverse methanogenesis have been proposed (Hoehler and Alperin, 1996), one of which was recently demonstrated *in vitro* (Scheller *et al.*, 2010).

Here, we address the first argument (i) of Hinrichs and colleagues that ANME-1 archaea are not methanogens operating in reverse, by presenting data on the occurrence and activity of ANME archaea in both

methane-oxidizing and methane-producing sediments. We applied RNA- and DNA-based analyses to brackish sediments of the White Oak River estuary, North Carolina, where the gene transcription patterns of ANME archaea can be observed in clearly separated zones of net methane production or oxidation. Since DNA can be stable in cold anoxic sediments on the order of 10^5 years (Willerslev *et al.*, 2004), its presence is not a sufficient indicator for active microorganisms. In contrast, RNA is much more readily degraded (Srivastava and Schlessinger, 1990), and is therefore a more specific biomarker for *in situ* metabolic activity.

Results

Geochemical depth distributions

Sulfate concentrations in brackish White Oak River estuary sediments (Fig. 1, column A) generally decrease from ~10 mM at the sediment–water interface to ~0.1 mM at depth. Sulfate : chloride ratios also decrease with depth (not shown), indicating that sulfate is consumed, presumably by the sulfate-reducing bacteria. We will refer to the sediment region where sulfate concentrations exceed 0.1 mM as the sulfate reduction zone.

Methane concentration profiles (Fig. 1, column A) have the characteristic sigmoidal shape that is common in marine sediments where molecular diffusion is the dominant transport process (Reeburgh, 2007). Methane concentrations are low (≤ 0.01 mM) throughout most of the sulfate reduction zone where sulfate concentrations are greater than 1 mM, increase rapidly with depth as sulfate becomes depleted, and remain relatively high (~1 mM) but variable towards the bottom of the core. Based on Fick's Second Law of Diffusion applied to porous sediments, the concave-up portion of the methane profile denotes the zone of net methane oxidation, the concave-down portion denotes the zone of net methane production, and the inflection point marks the boundary between methane oxidation and methane production zones (Berner, 1980).

An inverse model (Alperin *et al.*, 1988) provides estimates of net methane oxidation and production rates by quantifying curvature (i.e., the second derivative) in the methane concentration profile. The model predicts a subsurface maximum in net methane oxidation rate near the base of the sulfate reduction zone (Fig. 1, column B) as has been measured with ^{14}C-labelled methane in a wide variety of marine sediments (Reeburgh, 2007). The boundary between methane oxidation and methane production zones for each core (marked by the dashed horizontal lines in Fig. 1) is well constrained as the concentration profile is highly curved and the methane data are relatively smooth in this portion of the sediment column. In contrast, the upper boundary of the methane oxidation zone is less constrained as there is minimal curvature in the concentration profile in near-surface sediments.

The inverse model also predicts that rates of net methane production are highest just below the base of the methane oxidation zone and in most cases, decrease rather abruptly with depth (Fig. 1, column B). Our cores, however, may not have penetrated through the entire methane production zone. This limitation, combined with increased 'noise' in the methane concentration data at the bottom of the cores, makes it impossible to accurately constrain the shape of the methane production rate profile. The inverse model provides reliable estimates of the depth marking the top of the methane production zone as well as the depth-integrated methane production rate (which by mass-balance must equal the flux of methane into the methane oxidation zone plus the flux of methane that is buried deep below the methane production zone). Our methane concentration data, however, are insufficient to determine whether methane production is focused in a relatively narrow (~20 cm) zone just below the methane oxidation zone, or whether methane production occurs at slower rates over a broader depth interval. A multi-component reaction-transport model applied to this site (Martens *et al.*, 1998) is consistent with the latter case. This model – which uses the benthic flux of dissolved inorganic carbon and the sulfate depletion depth to constrain the quantity and reactivity of sedimentary organic matter – predicts that more than half of the depth-integrated methane production occurs at depths greater than 80 cm. Resolving which model best reflects the true methane production rate profile will require more data.

Depth distributions of δ^{13}C-methane were measured for two cores in July 2008 (Fig. 1, column E) and provide a check on the location of the lower boundary of the methane oxidation zone predicted by the inverse model. Methane oxidation causes the δ^{13}C-methane profile to shift towards 'heavier' (less negative) values at shallower depths (Fig. 1, column E) since ^{12}C-methane is preferentially oxidized as it diffuses up the core (Reeburgh, 2007). δ^{13}C-methane profiles predicted by an isotope reaction-transport model using the methane reaction rate profiles in Fig. 1 (column B) are consistent with the measured values. This confirms that net methane oxidation in these two cores does not occur at depths below 40 cm. The predicted kinetic isotope effect (α) for anaerobic methane oxidation (1.015 for Jul 08-1 and 1.019 for Jul 08-2) is within the range measured for enrichments of ANME-2 from three different methane seeps (1.012–1.039) (Holler *et al.*, 2009).

The methane reaction rate profiles derived from the geochemical data are consistent with our current understanding of the vertical zonation of organic matter remineralization in most anoxic marine sediments. In
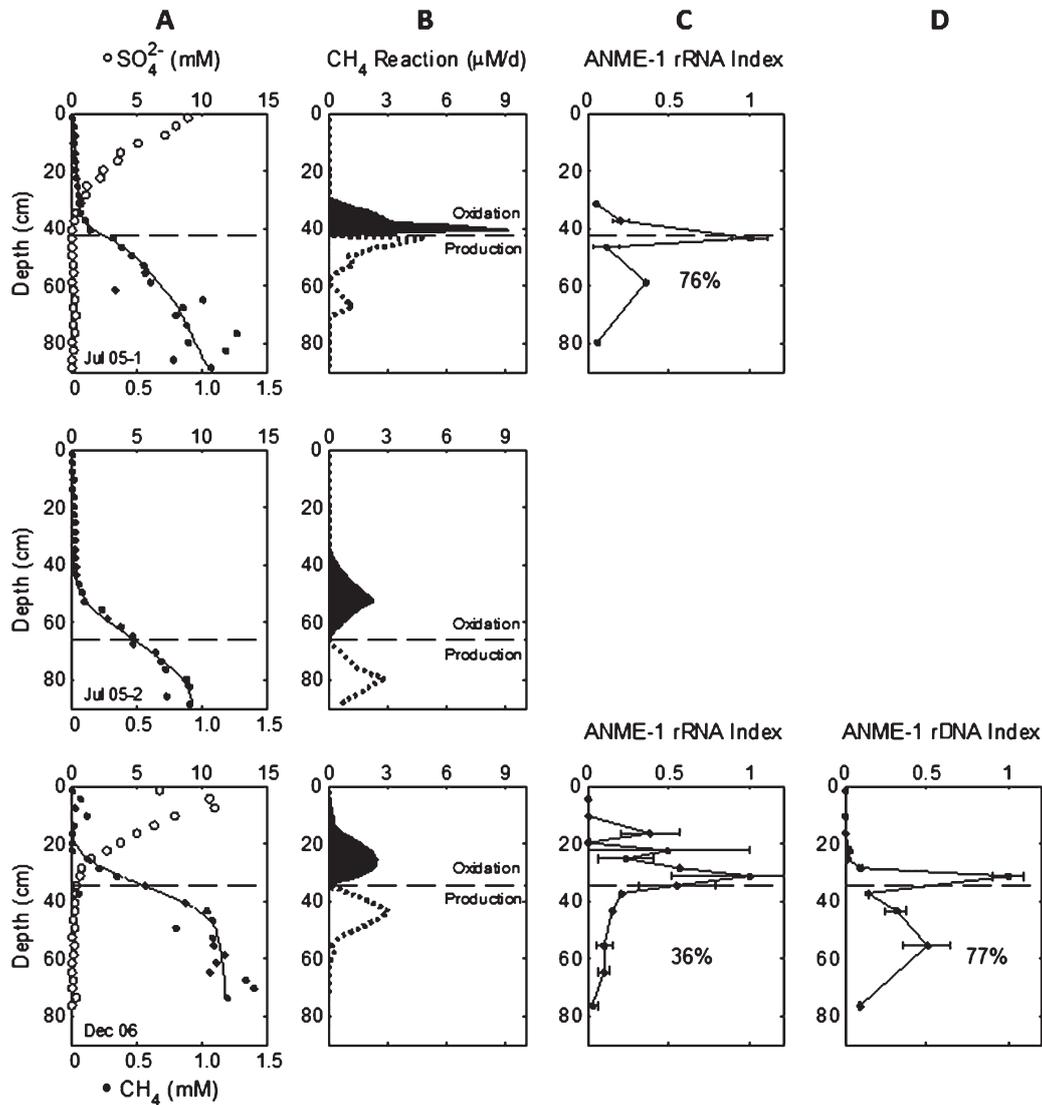
Fig. 1. Geochemistry and microbial depth distributions. Column A: Concentrations of methane (●) and sulfate (○), with methane concentrations predicted by a reaction-transport model (solid line) driven by rates shown in Column B. Column B: Methane oxidation rates (filled black area) and methane production rates (dotted line) estimated from an inverse model applied to the methane concentrations data, except for the case of cores Jul 08-1 and Jul 08-2, where $\delta^{13}C$-CH_4 data provide an additional constraint on the upper boundary of the methane oxidation zone. The small black arrows point to the lower boundary of the methane oxidation rate profile that is inferred from the $\delta^{13}C$-CH_4 data. The dotted lines for methane production rates denote that the shape of these profiles is not well-constrained because the deep methane data are 'noisy' and may not extend through the entire methane production zone. Columns C and D: ANME-1 16S rRNA index measured with RT-qPCR, and ANME-1 16S rDNA index measured with qPCR in copies per gram of sediment at each depth divided by the highest value of copies per gram of sediment for that core, with error bars representing the standard deviations of two to four measurements. Column E: $\delta^{13}C$ of methane, with profiles predicted by an isotope-reaction-transport model (solid line) for a kinetic isotope effect (α) for anaerobic methane oxidation of 1.015 (Jul 08-1) and 1.019 (Jul 08-2). Dashed horizontal lines indicate the depth of transition between methane oxidation and production zones. Cores, top to bottom, are Jul 05-1 (qPCR and $\delta^{13}C$ not measured), Jul 05-2 (RT-qPCR, qPCR and $\delta^{13}C$ not measured, but analysed for cDNA sequences and FISH), Dec 06 ($\delta^{13}C$ not measured), Jul 08-1 and Jul 08-2. The percentage of total depth-integrated copies of rRNA or rDNA that are present in the methane production zone are listed for each core. (continued on next page)

sulfate-containing sediments, sulfate-reducing bacteria out-compete methanogens for common substrates that are produced by organic matter fermentation, and maintain H_2 at very low concentrations (< 1 nM) (Lovley *et al.*, 1982; Hoehler *et al.*, 1998). In sulfate-depleted sediments, lack of competition from sulfate-reducing bacteria

allows methanogenic archaea to assimilate the fermentation products and convert them to methane (Hoehler *et al.*, 1994). The methane that diffuses upward from the methane production zone is nearly quantitatively oxidized near the base of the sulfate reduction zone where low H_2 concentrations make methane oxidation to CO_2
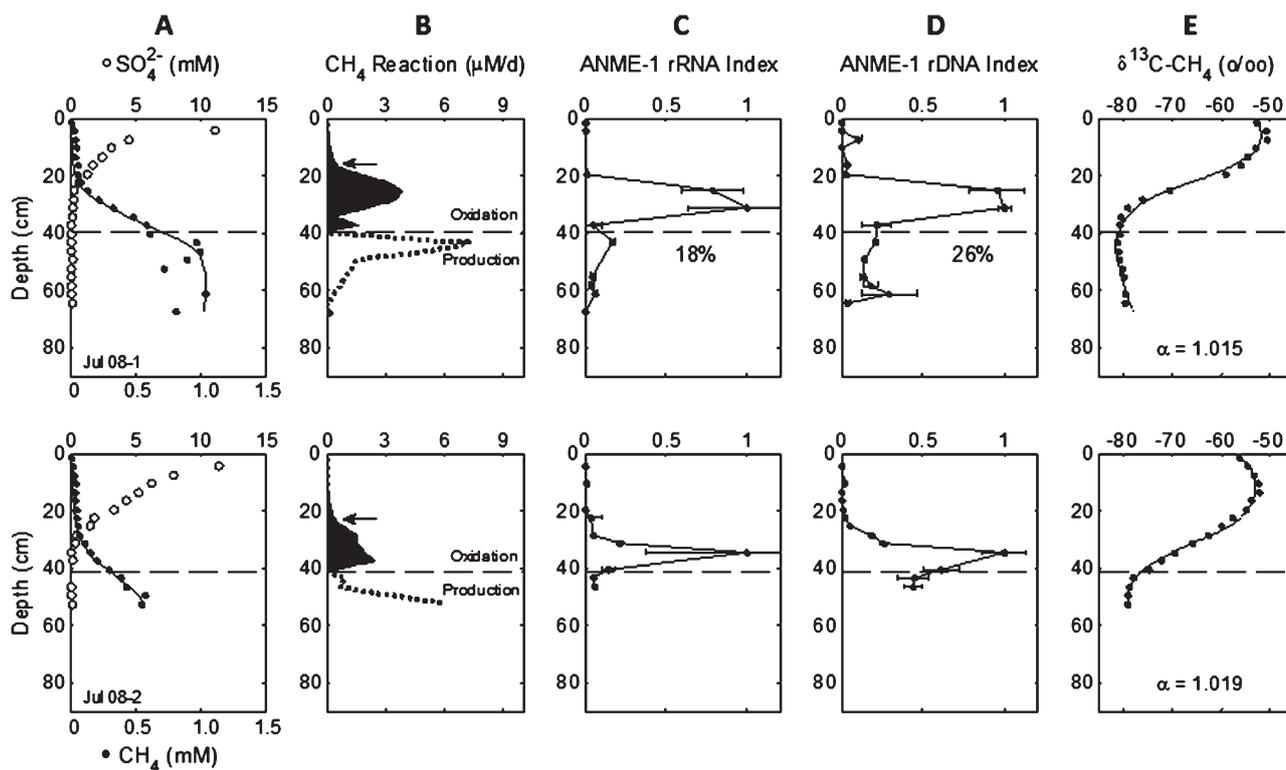
Fig. 1. *cont.*

and H$_2$ energetically favourable (Hoehler *et al.*, 1994; 1998).

Microbial depth distributions

Extraction of DNA and especially RNA from natural sediments makes absolute quantification difficult since extraction efficiencies can be variable and are difficult to measure accurately (Lloyd *et al.*, 2010). Therefore, 16S rRNA and 16S rDNA copy numbers are not reported as absolute quantities but are indexed to the highest average copy number per measurement type per core. That is, an index value of 1.0 marks the depth with the highest average rRNA or rDNA copy number per gram of dry sediment; an index of 0.5 marks the depth with half as many copy numbers.

The 16S rDNA and rRNA indices provide complementary information regarding the depth distribution of abundance and activity of ANME-1 archaea. The 16S rDNA index reflects the relative abundance of ANME-1 cells, since published genomes of environmental ANME-1 cells have one 16S rDNA copy per genome (Meyerdierks *et al.*, 2010), and this value is not expected to change much with growth rate. The 16S rRNA index reflects both the relative abundance and the activity of ANME-1 cells, since the number of ribosomes per cell is proportional to the cellular growth rate (Kemp *et al.*, 1993). Although the absolute

number of ribosomes per rDNA copy is biased by different extraction efficiencies for rRNA and rDNA and the addition of a reverse transcription step for rRNA (and possibly by the persistence of rDNA in dead cells), down-core variations in the ratio of ANME-1 rRNA:rDNA indices provide a proxy of relative changes in the growth rate of ANME-1 archaea with depth (lower values of rRNA:rDNA indicate relatively lower growth rates).

Profiles of ANME-1 16S rRNA and rDNA indices are shown in Fig. 1 (columns C, D). Both indices are generally low throughout much of the sulfate reduction zone where methane production suffers from competition from sulfate-reducing bacteria, and methane oxidation is limited by low methane concentrations (≤ 0.01 mM). As expected, both indices have a peak that coincides with the subsurface peak in methane oxidation rate, consistent with the widely held view that ANME-1 archaea are capable of anaerobic methane oxidation. The abrupt decline in both indices at the boundary between methane oxidation and methane production suggests that the abundance of ANME-1 archaea declines in this horizon, and that the persistent cells become dormant (the rRNA index – which indicates activity – approaches zero in three of the four cores). The sharp decline in the rDNA index suggests that in these sediments, 16S rDNA from ANME-1 archaea degrades on timescales of years. Thus, we consider the rDNA index to closely reflect the abundance of ANME-1 archaea living in

each depth interval rather than the cumulative mass of dead cells.

For the three cores that were analysed for gene transcription and that penetrated well into the methane production zone (Jul 05-1, Dec 06 and Jul 08-1), both rRNA and rDNA indices have non-zero values in methanogenic sediments (Fig. 1, column C, D). In fact, a majority of these profiles (Jul 05-1/rRNA, Dec 06/rDNA and Jul 08-1/ rRNA) show a clear secondary peak in the methane production zone. The rRNA and rDNA indices do not track the methane production rate profiles nearly as well as they track the methane oxidation rate profiles. This is not surprising given uncertainty in the shape of our methane production rate profiles stemming from insufficient data to define the base of the methane production zone and scatter in the methane concentration data towards the bottom of the core. Depth-integrating the rDNA index suggests that a sizable fraction (26–77%) of the whole-core ANME-1 population is present in the methane production zone. Depth-integrating the rRNA index suggests that a similar fraction (18–76%) of whole-core ANME-1 activity occurs below the methane oxidation zone. These values represent lower limits as the cores may not have penetrated through the entire methane production zone.

Three cores were analysed for both ANME-1 16S rRNA and rDNA (Dec 06, Jul 08-1, Jul 08-2). For all three of these cores, the rRNA index attenuates more quickly with depth than the rDNA index, suggesting that ANME-1 archaea grow faster in the methane oxidation zone than in the methane production zone. This implies that there is more metabolic power available to ANME-1 in the methane oxidation zone than in the methane production zone. The power available from a metabolic process is the product of the Gibbs free energy of reaction and the reaction rate. Studies of the energy requirements of methanogenesis (Hoehler *et al.*, 2001) and methane oxidation (Hoehler *et al.*, 1994) suggest that both processes are supported by similar energy yields (*c.* −10 to −15 kJ mol^{-1} CH$_4$). If methane production and consumption have comparable energy yields in these sediments, faster ANME-1 growth rates in the oxidation zone suggest that methane oxidation rates are higher, but focused in a relatively narrow depth interval, compared with methane production rates.

Our rRNA and rDNA data are consistent with the standard model of stratification of sulfate reduction linked to methane oxidation and methanogenesis (Hoehler *et al.*, 1994). A sharp decrease in rRNA and rDNA indices at the base of the methane oxidation zone is consistent with a region where neither methane oxidation nor methane production can support cellular energy requirements. Here sulfate-reducing bacteria become sulfate-limited and their rate of H$_2$ consumption cannot keep pace with H$_2$ generation via fermentation. A resulting increase in H$_2$ concen-

trations has been shown to halt anaerobic methane oxidation, presumably since reverse methanogenesis no longer provides the organism with a free energy gain (Hoehler *et al.*, 1994). As sulfate continues to decline, sulfate reducers decrease in activity, as shown by the inconsistent amplification of *dsrAB* mRNA (see below), and H$_2$ continues to rise until it eventually becomes high enough to support the minimum energy requirements of methanogens. The depth interval where neither methane oxidation nor production can support microbial maintenance energies has been called the 'no reaction' zone (Hoehler *et al.*, 1994).

Below the no reaction zone, rRNA and rDNA indices generally increase to a secondary peak within the methane production zone. Of the total depth-integrated rDNA and rRNA indices for each core, 26–77% of rDNA and 18–76% of rRNA are located in the methane production zone, indicating that substantial fractions of ANME-1 cell numbers and activity occur here. All these data are consistent with the notion that ANME-1 function as methanotrophs in the methane oxidation zone, and as methanogens in the methane production zone. This is consistent with the 'reverse methanogenesis' mechanism in which methanogens are able to switch their metabolism from methane production to methane oxidation depending on which process is thermodynamically favourable (Zehnder and Brock, 1979; Hoehler and Alperin, 1996). This hypothesis is based on the observation that cultured methanogens are able to oxidize methane to CO$_2$ while engaged in net methane production (Zehnder and Brock, 1979), and that net methane oxidation can be induced in methanogenic sediments by experimentally manipulating the H$_2$ concentration to make methane oxidation thermodynamically feasible (Hoehler *et al.*, 1994).

Clone libraries

General archaeal 16S rRNA clone libraries yielded ANME-1 archaea within the methane oxidation zone as well as at least 45 cm into the methane production zone (Table 1A), providing additional evidence that ANME-1 remain active in methanogenic sediments. These sequences grouped with other ANME-1 16S rRNA sequences derived from both methane seeps and diffusive sediments (Fig. S1). They did not form a separate White Oak River-specific clade, and did not have distinct clades between the methane oxidation and production zones. ANME-1 comprised a small (< 12%) part of archaeal 16S rRNA clone libraries, which were dominated by uncultured, benthic *Crenarchaeota* (data not shown).

A stringent test to detect metabolically active methane producers is the presence of *mcrA* mRNA, which has a lifetime of minutes once metabolic activity stops (Henni-

Table 1. cDNA clone library results, with archaeal 16S rRNA, *mcrA* mRNA and *dsrAB* mRNA.

A. 16S rRNA				
Core and depth	CH$_4$ oxidized or produced	Number of ANME-1 clones	Other methanogens (*n*)	Number of total clones
Dec 06 24–27 cm	Oxidized	3	ND	52
Jul 05-2 54–57 cm	Oxidized	7	ND	91
Jul 08-2 48–51 cm	Produced	4	ND	33
Jul 05-1 60–63 cm	Produced	3	ND	68
Dec 06 69–72 cm	Produced	2	ND	90
Jul 05-2 87–90 cm	Produced	5	ND	98

B. *mcrA* mRNA				
Core and depth	CH$_4$ oxidized or produced	Number of ANME-1 clones	Other methanogens (*n*)	Number of total clones
Jul 08-2 3–6 cm	Oxidized	12	ND	12
Jul 08-2 9–12 cm	Oxidized	26	ND	26
Jul 08-2 18–21 cm	Oxidized	30	ND	30
Jul 05-2 54–57 cm	Oxidized	18	ND	18
Jul 08-2 48–51 cm	Produced	36	ND	36
Jul 05-1 60–63 cm	Produced	24	Methanomicrobiales (19)	43
Jul 05-1 87–90 cm	Produced	2	Methanosaeta sp. (37)	39
Jul 05-2 87–90 cm	Produced	3	ND	3

C. *dsrAB* mRNA			
Core and depth	CH$_4$ oxidized or produced	Sulfate reducers (*n*)	Number of total clones
Dec 06 24–27 cm	Oxidized	Cluster B (32)	32
Jul 05-2 51–54 cm	Oxidized	Cluster B (72), *Desulfobacterium anilinii* (7)	79
Jul 05-1 60–63 cm	Produced	Cluster B (7)	7
Jul 05-1 84–87 cm	Produced	*Desulfobacca acetoxidans* (29)	29

ND stands for None Detected, and implies that a particular group was not represented in our clone library, not that it was necessarily absent in the sample.

gan and Reeve, 1994) and encodes the enzyme that catalyses the energy-conserving step in methanogenesis, methyl coenzyme M reductase. This enzyme is presumed to also mediate anaerobic methane oxidation since it is reversible (Scheller *et al.*, 2010). Within both the methane oxidation and production zones, *mcrA* mRNA specific for ANME-1 dominated *mcrA* clones (Table 1B). As with 16S rRNA, the ANME-1 *mcrA* grouped with sequences from methane seeps, without forming a separate clade; and no phylogenetic distinctions were seen between sequences from methane oxidation and production zones (Fig. 2A). In two out of four clone libraries within the methanogenic zone, *mcrA* mRNA from other methanogen-affiliated archaea (*Methanosaeta* sp. at 87–90 cm and members of the *Methanomicrobiales* at 60–63 cm in core Jul 05-1) were also identified (Table 1B; Fig. 2A). Non-ANME methanogens were recovered with methanogen-specific *mcrA* primers but not with three general archaeal 16S primers (Table 1A, Tables S1 and S2), indicating low numbers and activity below detection limits with archaeal 16S rRNA primers.

In the methane oxidation zone, *dsrAB* mRNA, which encodes dissimilatory sulfite reductase was reproducibly amplified (Table 1C). This enzyme is constitutively transcribed in sulfate-reducing bacteria while they are reducing sulfate as well as when they use a non-sulfate-reducing metabolism (Neretin *et al.*, 2003). *dsrAB* phylotypes in the methane oxidation zone grouped within the *Desulfobacteraceae* (Fig. S2); other members of the *Desulfobacteraceae* physically associate with ANME archaea in methane seep sites (Knittel and Boetius, 2009). In methanogenic sediments, *dsrAB* mRNA was amplified only sporadically (4 out of 29 attempts), with a significantly lower success rate than in the methane oxidation zone ($\chi^2 = 7.99$, d.f. = 1, $P > 98\%$, two-tailed Chi-squared test; Fig. S3). Sequences retrieved from two methanogenic depths grouped either within the *Desulfobacteraceae* or near *Desulfobacca acetoxidans*, an acetate-utilizing sulfate reducer. The low detection rate of *dsrAB* gene transcription was consistent with constitutive *dsrAB* transcription in small amounts, as in fermentative sulfate reducers (Neretin *et al.*, 2003).

CAtalysed Reporter Deposition Fluorescent *In Situ* Hybridization (CARD-FISH) with probes specific for ANME-1, ANME-2 and the *Desulfosarcinales/ Desulfosarcina* group showed that ANME-1 archaea in the methane oxidation zone existed only as single rods or small conspecific clusters containing ≤ 4 rod-shaped
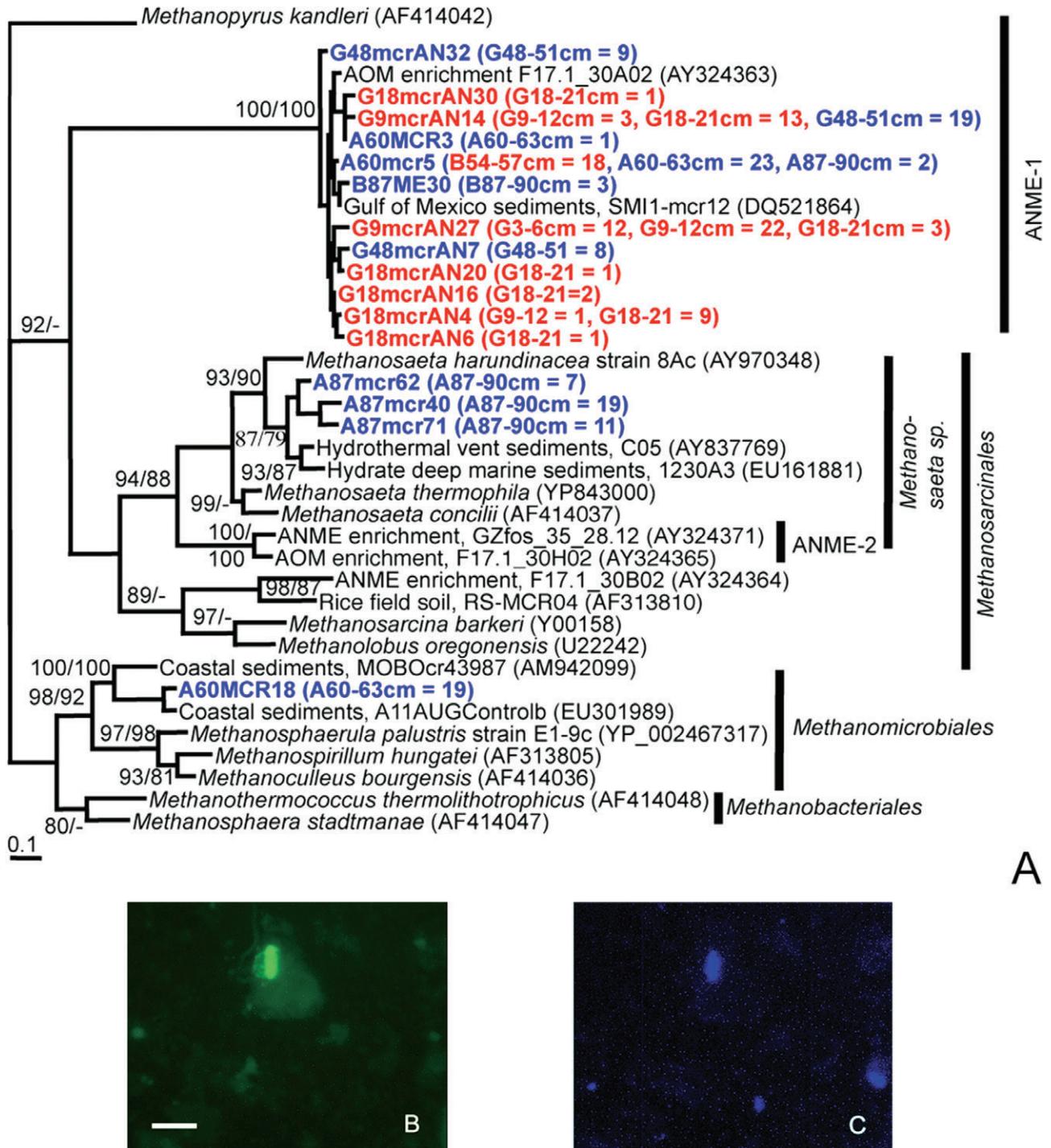
Fig. 2. Phylogeny of ANME-1 *mcrA* mRNA sequences and CARD-FISH photomicrograph of ANME-1.
A. Neighbour-joining tree of amino acid translations of *mcrA* mRNA cDNA, with distance- and then parsimony-based bootstrap support
(> 60%, 1000 repetitions) listed at the nodes. Numbers of clones represented by each 97% OTU group (determined from nucleic acids) are
shown in parentheses, using A for core Jul 05-1, B for core Jul 05-2, E for core Dec 06 and G for core Jul 08-2. Scale bar shows 10%
distance. Red clones are from the methane oxidation zone and blue clones are from the methane production zone.
B. CARD-FISH labelled with probe ANME-1-350 in green from core Jul 05-2 51–54 cm. Scale bar is 5 µm.
C. Blue DAPI signal from the same image.

cells, and did not physically associate with other phylotypes (Fig. 2B and C); the lack of associated bacteria is common for ANME-1, ANME-2 and ANME-3 archaea (Table 2). ANME-2 archaea were never detected with CARD-FISH. ANME-1 signals were only found in the methane oxidation zone (Jul 05-2 51–54 cm) using CARD-FISH. We note that cell densities were too low for accurate quantification using this method, since many fields of view had to be examined to find a single ANME-1 signal. Therefore, the lack of ANME-1 or ANME-2 signals in other depths (Jul 05-2, 0–3 cm, 3–6 cm, 9–12 cm, 18–21 cm, 42–45 cm, 72–75 cm and 87–90 cm) should not be taken as evidence for absence of ANME-1 or ANME-2.

Discussion

We have shown that ANME-1 archaea are present and active in sediments from the White Oak River estuary at depths where there is net methane oxidation and also at depths where there is net methane production. We found ANME-1-specific 16S rRNA and *mcrA* mRNA, molecules that are rapidly degraded in non-metabolically active cells, in both of these two sedimentary zones. The rDNA index (a proxy for ANME-1 cell number) and the rRNA index (a proxy for ANME-1 metabolic activity) increase within the methane oxidation zone, decrease at the base of the methane oxidation zone, and then generally increase to a secondary peak within the methane production zone. Of the total depth-integrated rDNA and rRNA indices for each core, 26–77% of rDNA and 18–76% of rRNA are located in the methane production zone, indicating that substantial fractions of ANME-1 cell numbers and activity occur here. All these data are consistent with the notion that ANME-1 in these sediments function as methanotrophs in the methane oxidation zone, and as methanogens in the methane production zone.

Evidence that ANME archaea are capable of methanogenesis comes from the substantial similarities they share with cultured methanogens such as phylogenetic affiliations, predicted gene functions, habitat ranges, morphologies and aggregation habits. 16S rRNA phylogeny places ANME-1 among the methanogens, and ANME-2 and ANME-3 within the methanogenic Order *Methanosarcinales*, with ANME-3 grouping within the genus *Methanococcoides* (Fig. S1). All cultured members of all five Orders of methanogens have been shown to produce methane (Boone *et al.*, 1993). The genomes of ANME-1 and ANME-2 have been sequenced from environmental samples and contain homologous genes for enzymes involved in all seven steps of methanogenesis, although one enzyme (N^5,N^{10}-methenyltetrahydromethanopterin

reductase) was not assigned to ANME-1 (Meyerdierks *et al.*, 2010). ANME-1 archaea also contain genes encoding the same carbon fixation pathway as cultured methanogens (Meyerdierks *et al.*, 2010). ANME-2 archaea have been shown to fix nitrogen (Dekas *et al.*, 2009), as do cultured methanogens in the *Methanosarcinales* (Murray and Zinder, 1984), and ANME lipid structures are very similar to those of cultured methanogens (Elvert and Suess, 1999; Hinrichs *et al.*, 1999). Microbial mats containing ANME archaea have been shown to express methyl coenzyme M reductase (Krüger *et al.*, 2003), an enzyme found in all orders of cultivated methanogens (Luton *et al.*, 2002), and its evolutionary path in ANME archaea mirrors that of cultured methanogens (Hallam *et al.*, 2003). ANME archaea fluoresce blue-green under ultraviolet light (Michaelis *et al.*, 2002; Knittel *et al.*, 2005; Lösekann *et al.*, 2007), a characteristic of cultured methanogens due to the presence of an F_{420} flavin-derived coenzyme. ANME archaea are often found alongside cultured methanogens at deep-sea biogenic methane seeps (Lanoil *et al.*, 2001) and in methane-producing marine sediments (Table 3, and references therein). At methane seeps with high organic matter, ANME archaea are often found in clusters with sulfate reducers (Boetius *et al.*, 2000), a trait shared with methanogens and sulfate reducers in high organic matter wastewater bioreactors (Santegoeds *et al.*, 1999). ANME-2 and ANME-3 often appear as coccoid cells and form clusters (Orphan *et al.*, 2002), as do cultured methanogens of the *Methanosarcinales* (Boone *et al.*, 1993); and ANME-1 are often rod-shaped (Orphan *et al.*, 2002), as are cultured methanogens of the *Methanobacteriales* and *Methanomicrobiales* (Boone *et al.*, 1993). Methane production has been demonstrated in ANME-rich methane seep sediments (Orcutt *et al.*, 2008), hydrocarbon-contaminated sediments (Siegert *et al.*, 2010) and microbial mats (Pimenov *et al.*, 1997; Seifert *et al.*, 2006; Treude *et al.*, 2007).

Despite the remarkable genetic, metabolic, structural and ecological similarities between uncultured ANME and cultured methanogenic archaea, it is widely assumed that ANME archaea are obligate methanotrophs that cannot gain energy from methane production. This assumption can be traced back to Hinrichs and colleagues who preferred obligate or dominant methanotrophy for ANME-1 largely on the grounds that ANME-1 archaea had never been detected in sediments where methane production was known to be active (Hinrichs *et al.*, 1999). Our results from the White Oak River estuary show the presence and activity of ANME-1 archaea in methanogenic sediments. At least five other studies (Table 3) found DNA from ANME archaea in methanogenic sediments, suggesting that our findings are not unique to one environment.

Table 2. Observations of physical associations of ANME-1, ANME-2 and ANME-3 with sulfate-reducing bacteria (With SRB), other bacteria (With Bac) or no other organisms (Alone) made using Fluorescence *In Situ* Hybridization (FISH).[a]

Type of environment	Location	ANME-1			ANME-2a/b and ANME-2c			ANME-3		
		With SRB[b]	With Bac[c]	Alone[d]	With SRB[b]	With Bac[c]	Alone[e]	With SRB[b]	With Bac[c]	Alone[e]
Methane seeps	Black Sea mats	1, 5, 15			3, 15	3	3			
	Eel River Basin	11	11	11, 16	10–12, 16, 18	11, 12	11,16 18			
	Gulf of Mexico	9	9	9	9, 13	13	9			
	Hydrate Ridge			3	3		3			
	Eastern Mediterranean			8	7, 8	8, 13				7, 8
	North Sea			17	13		13[f]			
	Haakon Mosby Mud Volcano			4	4			4, 6	4, 13	4
Seasonal methane seep	Eckernforde Bay			14			14			
Freshwater	Lake Plußsee freshwater			2			2			
Marine non-seep	White Oak River estuary			This study						

a. Listed are reference numbers for the studies where these aggregations (or lack thereof) are documented. This table is not exhaustive; there may be other reports that are not included. Empty cells should not necessarily be taken as evidence for the absence of a certain aggregation behaviour for a certain type of ANME at a certain location since some studies only focused on a subset of cell types.
b. This category includes spherical clusters of ANME cells on the inside, surrounded by sulfate-reducing bacterial cells, mats of ANME cells pock-marked with sulfate-reducing bacterial cells, and mixed clusters where ANME cells and sulfate-reducing bacterial cells appear evenly distributed.
c. Except for Pernthaler and colleagues (2008), where the bacteria were identified as *Alphaproteobacteria* and *Betaproteobacteria*, the identities of these bacteria are unknown.
d. This category includes long filaments of rod-shaped ANME-1 cells or single ANME-1 rods.
e. This category includes spherical clusters of monospecific ANME-2 or ANME-3 cells or single ANME-2 cells or single ANME-3 cocci.
f. The authors concluded that single ANME-2 cells were the result of sonication before hybridization.
Data sources: [1](Blumenberg *et al.*, 2004), [2](Eller *et al.*, 2005), [3](Knittel *et al.*, 2005), [4](Lösekann *et al.*, 2007), [5](Michaelis *et al.*, 2002), [6](Niemann *et al.*, 2006), [7](Omoregie *et al.*, 2008), [8](Omoregie *et al.*, 2009), [9](Orcutt *et al.*, 2005), [10](Orphan *et al.*, 2001), [11](Orphan *et al.*, 2002), [12](Pernthaler *et al.*, 2008), [13](Schreiber *et al.*, 2010), [14](Treude *et al.*, 2005), [15](Treude *et al.*, 2007), [16](House *et al.*, 2009), [17](Niemann *et al.*, 2005), [18](Orphan *et al.*, 2001).

Table 3. Methanogen-like archaea found in sediments where zones of methane oxidation and production have been clearly defined.

Location	Evidence for methane oxidation/production	Evidence for microorganisms	Methanogen-like archaea in methane oxidation zone	Methanogen-like archaea in methane production zone	Reference
Colne Point salt marsh, Essex, UK	$^{14}CO_2$ converted to $^{14}CH_4$ and CH_4 efflux into overlying water column	16S rDNA	Not examined	*Methanomicrobiales* ANME-2a/b[a] and other *Methanosarcinales*	Senior *et al.* (1982); Munson *et al.* (1997)
Aarhus Bay, Denmark	Modelled rates and curve of CH_4 profile	16S rDNA	ANME-1, ANME-2 and other *Methanosarcinales*	Amplification with ANME-1-specific primer	Thomsen *et al.* (2001)
Skan Bay, Alaska, USA	Radiotracer rates and curve of CH_4 concentration and $δ^{13}C$ profiles	16S rDNA	ANME-1, ANME-2 and other *Methanosarcinales* *Methanomicrobiales*	ANME-2	Kendall *et al.* (2007)
Skagerrak Bay, Denmark	Radiotracer rates and curve of CH_4 concentration profile	16S rDNA	Not examined[b]	ANME-2a and other *Methanosarcinales* *Methanomicrobiales*, ANME-3	Parkes *et al.* (2007)
Santa Barbara Basin, California, USA	Curve of CH_4 concentration profile	16S rDNA	ANME-1	ANME-1	Harrison *et al.* (2009)
White Oak River estuary, North Carolina, USA	Modelled rates, curve of CH_4 concentration and $δ^{13}C$ profiles	16S rRNA, *mcrA* mRNA, 16S rDNA	ANME-1	*Methanosarcinales*[c] *Methanomicrobiales*[c]	Current study

a. These clones (2MT7 and 2C83 for ANME-2a) were recovered before Boetius and colleagues named the ANME-2 group in 2000 (Boetius *et al.*, 2000).
b. Methane concentration profiles and radiotracer rates are in good agreement that net methane oxidation takes place between ~0.5 and 0.8 m. No 16S rDNA analysis was performed for this depth interval.
c. Found only with *mcrA* mRNA.

Another key argument by Hinrichs and colleagues (1999) that methane oxidation is the only process that could account for the extreme ^{13}C-depletion ($δ^{13}C ≤ −100‰$) observed in lipids attributed to ANME-1 archaea (Hinrichs *et al.*, 1999) also merits re-evaluation. They assumed that methanogenic archaea produce lipids with a $δ^{13}C$ of −30‰, based on the δ value measured for methanogenic biomarkers in an Eocene lake shale with estimated porewater $δ^{13}C$-CO_2 = +1‰; temperature = 25°C (Hayes *et al.*, 1987). Recent experimental (Londry *et al.*, 2008) and theoretical (Alperin and Hoehler, 2009) studies show that under conditions common to deep-sea methane seeps with porewater $δ^{13}C$-CO_2 ~ −40‰; temperature < 10°C (Alperin and Hoehler, 2009), normally functioning methanogens can produce lipids that are extremely depleted in ^{13}C.

Evidence that ANME archaea are obligate methanotrophs

The assumption that ANME archaea are obligate methanotrophs remains pervasive (Knittel and Boetius, 2009), sustained by two publications which provide experimental evidence suggesting that ANME archaea are not capable of net methane production. We discuss both studies below and show that neither one is definitive.

Treude and colleagues found that the conversion of ^{14}C-labelled bicarbonate to methane in 9- to 32-day incubations of ANME-rich microbial mats from the Black Sea required the presence of methane in the headspace, and that methane production was not stimulated by adding H_2 and/or removing sulfate (Treude *et al.*, 2007). Therefore, the authors surmised that methane production only occurred as a back-reaction of methane oxidation. They concluded that Black Sea mats do not contain any organisms that are capable of net methane production, implying that the ANME archaea are obligate methanotrophs. These results, however, conflict with an earlier study (Seifert *et al.*, 2006) where mat material collected from the same location and during the same expedition produced methane with a consistent carbon isotopic composition (−81 ± 1‰) when incubated without methane in the headspace. Furthermore, Seifert and colleagues (2006) found that methane production rates were stimulated by adding H_2 (9.4 ± 2.3 [+H_2] versus 7.0 ± 1.5 [control] $μmol\ g_{dw}^{-1}$ day^{-1}; $P > 80\%$, *t*-test) as well as other methanogenic substrates. Further study is needed to explain the divergent results from these two studies.

Orcutt and colleagues (2008) conducted an experiment to determine whether methane production in sulfate-rich Gulf of Mexico sediments, which contained significant ANME-1 cells, could be stimulated by elevating the H_2 concentration (Orcutt *et al.*, 2008). Sediment was slurried

with sulfate-rich seawater medium, purged with CH_4 or N_2 and injected with H_2 to give an initial concentration of 2.5%. Slurries were incubated for 68 days during which time there was no medium exchange and no replenishment of headspace gases. After the incubation, aliquots of slurry were injected with ^{14}C-labelled bicarbonate to measure methane production rates. Orcutt and colleagues found that the addition of H_2 at the start of the incubation (rates were not measured at this time) did not stimulate methane production after the incubation when rates were measured. The results of this H_2-amendment experiment should be viewed as preliminary for two reasons. First, similar sediments from this site have a substantial clone library representation of methanogens in the order *Methanomicrobiales* (Mills *et al.*, 2003), most cultured representatives of which are capable of hydrogenotrophic methanogenesis (Boone *et al.*, 1993). The inability to demonstrate H_2-dependent methanogenesis is inconsistent with the likely presence of hydrogenotrophic methanogens in the slurries. The second reason that the H_2-amendment experiment is inconclusive is that anoxic marine sediments contain a wide variety of microorganisms that are able to consume H_2 (Fenchel *et al.*, 1998). Since the H_2 concentration at the end of the 68-day incubation period was not reported, it is not possible to determine to what extent, if any, the H_2 concentration during the rate measurement was elevated relative to the background level.

Conclusions

The coordinated geochemical and microbiological data in the White Oak River estuary show that ANME-1 archaea are present and active in both methane-oxidizing and methane-producing sediments. Explaining the persistence and gene transcription activity of ANME-1 archaea in methanogenic sediments as obligate methanotrophs would require invoking untested mechanisms for concurrent energy yields by methane production and oxidation in a single sediment depth. Further, an unknown electron acceptor would have to be as available and abundant in the methane production zone as is dissolved sulfate in the methane oxidation zone. These problematic assumptions become superfluous once the White Oak River data are interpreted parsimoniously as evidence for methanogenic capability in ANME-1 archaea.

A model in which ANME-1 switch between methane oxidation in the methane oxidation zone and methane production in the methane production zone is consistent with all current data and agrees with the observed geochemistry. This model does not require extraordinary preservation of electron acceptors, discoveries of novel genes to allow methane oxidation and sulfate reduction in a single organism, or assumptions of chemical compart-

mentalization via microniches or interspecies electron transfer through extracellular structures. Reversible methanogenesis in ANME archaea is consistent with the distribution of ANME archaea in other marine sediments (Table 3), the phylogenetic and structural similarities of the ANME archaea to cultured methanogens, the presence of genes and proteins in the methanogenic enzymatic pathway (Hallam *et al.*, 2004; Pernthaler *et al.*, 2008; Meyerdierks *et al.*, 2010), the propensity for ANME archaea to exist with and without a bacterial partner (Table 2), and highly ^{13}C-depleted biomass (Londry *et al.*, 2008; Alperin and Hoehler, 2009). When one considers the patterns observed as well as the thermodynamic constraints within the various horizons, methanogenic capability by ANME-1 archaea in deep sediments becomes a compelling explanation. Thus, the assumption that ANME-1 archaea are reliable proxies for anaerobic methane oxidation should be re-examined.

Experimental procedures

Sample collection

Five ~1 m plunger cores were collected from ~1.5 m water depth in brackish waters in the White Oak River estuary, near Stella, North Carolina (34°44.490′N, 77°07.44′W; Fig. S4) in July 2005 (Jul 05-1 and Jul 05-2, ~3 m apart, 28°C), December 2006 (Dec 06, 11°C) and July 2008 (Jul 08-1 and Jul 08-2, ~3 m apart, 28°C). Cores were transported to the laboratory in Chapel Hill, sectioned into 3 cm intervals at *in situ* temperature, and subsampled for geochemical and molecular biological measurements. The approximate time elapsed between core collection and processing was 72 h (Jul 05-1), 96 h (Jul 05-2), 48 h (Dec 06), 24 h (Jul 08-1) and 72 h (Jul 08-2). We suspect that these delays contributed to scatter in methane concentrations near the bottom of the core. Aliquots of sediment were also fixed with 3% formaldehyde for 4–5 h at 2°C, washed twice with phosphate-buffered saline (PBS) and stored at −20°C in a 1:1 PBS : ethanol mixture.

DNA and RNA extractions

RNA extraction details for each depth are listed in Table S1, using the published protocols listed. For cores Jul 05-1, Jul 05-2 and Dec 06, RNA destined for clone libraries underwent purification with RNeasy MinElute (Qiagen), DNA degradation with DNase I (Ambion) at 37°C for 30 min and repurification with RNeasy MinElute to remove DNase enzymes. RNA and DNA from cores Jul 05-1 and Dec 06 destined for quantitative PCR (qPCR) and quantitative RT-PCR (RT-qPCR) were purified via polyacrylamide gel as described previously (Lloyd *et al.*, 2010), followed by two 30 min 37°C incubations with TurboDNase (Ambion) with DNase removal via deactivation reagent (Ambion). For cores Jul 08-1 and Jul 08-2, RNA destined for clone libraries and RT-qPCR were incubated at 37°C for 30 min with TurboDNase (Ambion) and deactivated with the Ambion reagent.

RT-PCR

Total RNA was used for reverse transcription and PCR with primers targeting archaeal 16S small-subunit rRNA or mRNA of *dsrAB* or *mcrA* (Table S2). In order to check for potential DNA co-extraction, each batch of extracted RNA was tested by PCR, using the same primer sets as for clone libraries. In each case, no bands were visible. The only exception was Jul 05-2, 87–90 cm, which was not checked for DNA co-extraction, although it was processed identically to other samples that had no DNA co-extraction in any of the primer sets used. As an additional precaution for the *mcrA* mRNA amplifications, triplicate PCR amplicons without reverse transcriptase (invisible in agarose gel) for core Jul 05-2, 54–57 cm, were cloned and 47 sequences were analysed, but did not contain *mcrA*.

Each 25 µl of RT-PCR reaction contained 1 µl of RNA template, 0.15 µl of each primer solution (100 µM), 1 µl of bovine serum albumin (10 mg ml⁻¹), as well as the following products from the Takara OneStep RT-PCR kit Version 2.0: 12.5 µl of buffer, 0.5 µl of RNase inhibitor, 0.5 µl of hot start *ExTaq* and 0.5 µl of reverse transcriptase. Each 25 µl of nested PCR reaction contained 1 µl of cDNA template, 0.15 µl of each primer solution (100 µM), 1 µl of bovine serum albumin (10 mg ml⁻¹), 4 µl of deoxynucleotide triphosphate (2.5 mM each dATP, dCTP, dGTP and dTTP), 2.5 µl of 10× FastBuffer I (Takara) and 0.125 µl of hot start SpeedStar *Taq* (Takara).

Conditions for RT-PCR in a Bio-Rad iCycler (Hercules, CA) were as follows: reverse transcription at 42°C for 5 min, reverse transcriptase inactivation and HotStar *Taq* activation at 95°C for 2 min, followed by 25 cycles for archaeal 16S rRNA cDNA and 40 cycles for *dsrAB* mRNA cDNA and *mcrA* mRNA cDNA, each consisting of 5 s denaturation at 95°C, 15 s at primer annealing temperature (listed in Table S2) and 20 s elongation at 72°C. The following protocol was used for nested PCR: 94°C polymerase activation for 2 min, followed by 40 cycles for *dsrAB* and 30 cycles for all others of 98°C denaturation for 10 s, annealing for 15 s (see Table S2 for temperatures) and 72°C extension for 20 s plus a final elongation at 72°C for 10 min. For some samples multiple RT-PCR runs for each primer combination were combined, cloned and sequenced (Table S1). Co-extracted blanks never resulted in RT-PCR-amplified material visible on a 1.5% agarose gel. All PCR and RT-PCR products were purified using either a MoBio PCR Clean-up kit or purification in a 1% agarose gel and MoBio UltraSpin for gel extraction.

Cloning, sequencing and sequence analysis

Purified products were cloned using the TOPO TA PCR cloning kit (Invitrogen, San Diego, CA), and transformed into *Escherichia coli* by electroporation. Sequences were obtained at the Josephine Bay Paul Center at the Marine Biological Laboratory (Woods Hole, MA), using an ABI 3730 sequencer, or at Genewiz (South Plainfield, NJ) on an ABI Prism 3730xl sequencer. Vector sequences were removed and forward and reverse reads were assembled into contigs using Sequencher 4.7 (GeneCodes). Chimeras were identified with PinTail (Ashelford *et al.*, 2006) and removed. CLUSTALW-aligned sequences were grouped into operational

taxonomic units of 97% similarity using an average of nearest and farthest neighbour joining in Mothur (a free program combining the programs SONS and DOTUR) (Schloss and Handelsman, 2005; 2006). Archaeal 16S rRNA sequences representative of each OTU were aligned against the 2007 Silva release (Pruesse *et al.*, 2007) with ARB (Ludwig *et al.* 2004). Neighbour-joining trees of 16S alignments (excluding the unalignable helix #6) and amino acid translations of the mRNA alignments were made using Paup (Swofford, 2000) and a *dsrAB* alignment database in Arb (Loy *et al.*, 2009). GenBank accession numbers are HQ651845–HQ651850.

Quantitative PCR and RT-PCR

Quantitative PCR and RT-qPCR were performed with SybrGreen detection on a Stratagene Mx3005P for all cores except Jul 08-1, for which a Roche Light Cycler was used. All amplifications were checked for specificity with dsDNA melt curves and any exhibiting multiple products were not considered in the analysis. The RT-qPCR products of three samples were cloned and sequenced to check for amplification of non-target cDNAs. Core Jul 08-2, 9–12 cm had one RT-qPCR product out of 30 sequenced that was not ANME-1, core Jul 05-1, 42–45 cm and core Jul 05-1, 57–60 cm each amplified only ANME-1 (24 fragments sequenced for each).

Since ANME-1 archaea have not yet been cultured, DNA standards were made from TOPO 2.1 plasmids (Invitrogen) containing an insert of a near-complete, PCR-amplified ANME-1 16S rRNA (Polz and Cavanaugh, 1997). RNA standards were *in vitro* transcribed from the same plasmid used for DNA, by cutting with SpeI (New England Biolabs), transcribing with T7 polymerase (TaKaRa) and purifying with the RNeasy MinElute kit. DNA standards were quantified with PicoGreen and RNA standards were quantified with RiboGreen on a Stratagene Mx3005P or Roche Light Cycler. For core Jul 08-1, RNA and DNA standards were also measured with absorbance at 260 nm using a NanoDrop spectrophotometer, and the results were within the replicate variability using the Ribogreen and Picogreen measurements (average deviation within triplicates was 6.5% from the mean). The reverse primer used for reverse transcription and SYBR-Green qPCR measurements was ANME-1-830r (Table S2) (Boetius *et al.*, 2000). The forward primer was modified from ANME1-632 reported in Boetius and colleagues (2000) to better match the ANME-1 sequences derived from the clone libraries, while still encompassing most ANME-1 16S rRNA sequences in the 2007 release of the Silva database (Pruesse *et al.*, 2007). The resulting primer has at least one mismatch to all non-ANME-116S sequences and is named ANME-1-628f because it is shifted four positions towards the 5′ end (Table S2).

Primer concentrations were chosen to minimize the quantification cycle, or Cq, of the standard, while also minimizing primer-dimers and non-target amplification, as assessed through post-amplification dsDNA melt curves. Each 25 µl of reaction contained 1 µl of DNA or RNA template at the appropriate dilution (see below), 12.5 µl of QuantiFast PCR or RT-PCR master mix containing SYBR-Green (Qiagen), 0.20 µl of ANME1-628f (10 µM) and 0.24 µl of ANME-1-830r (10 µM) [except for core Jul 08-1 which used 0.20 µl of the

reverse primer], and 0.25 µl of QuantiFast reverse transcriptase (mixture of Sensiscript and Omniscript) for RT-qPCR. The RT-qPCR protocol included the following steps: 50°C incubation for reverse transcription for 10 min, 95°C polymerase activation for 5 min, followed by 40 cycles of 95°C denaturation for 10 s and 60°C annealing for 45 s, followed by a melt curve from 95°C to 55°C. The qPCR protocol was identical, minus the initial 50°C step. Stratagene MxPro or Roche Light Cycler software was used to determine the Cq of each reaction using a single threshold fluorescence level and the efficiency of each standard curve (all were > 90%). For each core and extraction method, samples were diluted until the Cq decreased log-linearly with sample dilution, indicating the absence of inhibition effects. This dilution factor was 50× for cores Jul 05-1, Dec 06 rRNA and Dec 06 rDNA; 10× for cores Jul 08-1 rRNA, Jul 08-1 rDNA and Jul 08-2 rRNA; 25× for core Jul 08-2 rDNA. For samples where no Cq could be determined, or where amplification occurred only through primer dimers (temperature around 80°C), the points were plotted on the *y*-axis of Fig. 1 (columns C and D) and can be assumed to be below the detection limit of our methods. Samples that had melt curves with a peak for the target amplicon as well as peaks for non-target amplicons or primer dimers were left out of the analysis altogether since they were neither accurately quantifiable nor below the detection limit. Extraction blanks as well as RNA samples without reverse transcriptase treatment all had Cq's of more than five cycles higher than the samples, indicating negligible contributions of contamination from extraneous nucleic acids or from DNA. All standard curves of Cq versus template concentration were fit with log-linear plots and had R^2 values of at least 0.98.

CARD-FISH protocol

Sediments were hybridized to probes (Table S2) following the methods of Lösekann and colleagues (2007). Sediments were sonicated at 20% power for 40 s to loosen cells from sediments, diluted 40-fold into PBS, filtered onto a 0.45 µm polycarbonate filter and covered in 0.01% low-melting-point agarose. Cells were permeabilized with Triton X (1% v/v in Milli-Q water) for Eub I–III and Arc915, Proteinase K (10 mg ml^{-1} in TE) for ANME1-350 and EelMS932, and lysozyme (10 mg ml^{-1} in TE) for DSS658; see Table S2 for hybridization conditions.

Porosity

Sediment water content was measured after drying sediment at 80°C for a few weeks. Porosity (φ) was calculated using the following formula:

$$\varphi = \frac{m_w/\rho_w}{m_w/\rho_w + \left(\dfrac{m_d - S*m_w/1000}{\rho_{ds}}\right)} \quad (1)$$

where m_w is the mass of the water lost on drying, m_d is the mass of the dried sediment, ρ_w is the density of pure water (defined as 1), ρ_{ds} is the density of dry sediment (assumed to be 2.5 g cm^{-3}; Benninger and Martens, 1983), and S is salinity in grams per kilogram (calculated from chloride concen-

trations measured by ion chromatography). Porosity values averaged 0.81 ± 0.02 and did not show a consistent variation with depth or between cores.

Porewater measurements

For sulfate measurements, plastic 15 ml tubes filled completely with sediment were centrifuged and the resulting porewater was filtered at 0.2 µm, acidified with 10% HCl and measured using a 2010i Dionex ion chromatograph (Sunnyvale, CA) with a Dionex OnGuard-Ag pre-filter to remove chloride ions. Core Jul 05-1 samples were not acidified after centrifugation before mixing with eluent, and chloride removal columns were not used for this core, or for core Dec 06. Some re-oxidation of sulfide occurred during the sulfate measurements for core Jul 05-1. This amount (0.65 ± 0.25 mM) was quantified through quadruplicate parallel samples measured with and without acidification, and subtracted from the original sulfate measurements. For a small number (~10%) of samples, the blank correction resulted in negative values which are plotted as zero in Fig. 1 (column A). For methane measurements, 4 ml or 3 ml of sediments were taken via cut-off syringe immediately after each section was sliced and quickly added to 60 ml serum vials containing 1 ml of 0.1 M KOH, which were stoppered and crimp-sealed with butyl rubber stoppers to minimize gas loss. After being shaken for 1 min to release methane from sediments (> 99.5% of the methane equilibrated in the headspace), a 5 ml headspace aliquot was displaced with an equal volume of anaerobic distilled water, injected into a 1 ml sample loop, and then analysed on a Shimadzu Mini II gas chromatograph (Kyoto, Japan) equipped with flame ionization detector. The detector was calibrated using commercial standards containing known partial pressure of methane. Methane concentrations for some depths for core Jul 08-1 (33–36, 36–39, 39–41, 41–44, 48–51, 51–54 and 60–63 cm) and Jul 08-2 (36–39, 42–45 and 48–51 cm) were quantified using methane peak areas from the isotope ratio mass spectrometer calibrated with samples where methane concentrations were also measured by GC. Methane concentrations (mmol per litre of porewater) were calculated using the following equation:

$$[CH_4] = \frac{p(CH_4)V_{headspace}}{RT\varphi V_{sed}1000}, \quad (2)$$

where $p(CH_4)$ is the partial pressure of methane (in ppmv), $V_{headspace}$ is the volume of the serum vial headspace (ml) after the sediment and KOH are added, R is the universal gas constant, T is the temperature at time of measurement in Kelvin and V_{sed} is the volume (ml) of whole sediment added to the serum vial. In addition, methane concentrations were divided by a small correction factor to account for the methane remaining in the dissolved phase during extraction (Vheadspace/(Vheadspace*Vsed*porosity*β)), where β is the Bunsen solubility coefficient at 27 psu and 25°C (Yamamoto *et al.* 1976). This correction was 0.997.

Stable carbon isotope ratios (expressed in standard δ-notation) were measured using an isotope ratio mass spectrometer coupled through a combustion interface to a gas chromatograph. For samples with > 0.1 mM methane, $\delta^{13}C$ values were measured via direct injection of the gas head-

space of basified sediments. Samples with smaller amounts of methane were cryo-focused in a liquid nitrogen-ethanol slush in order to allow the injection of 0.5 ml, or 5 ml gas headspace from each sample.

Reaction-transport models

The sediment depth distribution of methane may be described by the following equation (Berner, 1980; Ullman and Aller, 1982):

$$\varphi^2 D \frac{d^2c}{dx^2} - \omega \frac{dc}{dx} + \Sigma R = 0, \qquad (3)$$

where φ is sediment porosity (0.8), D is the molecular diffusion coefficient for methane [1.83×10^{-5} cm^2 s^{-1} at 28°C and 10 psu (cores Jul 05-1 and Jul 05-2) or 1.13×10^{-5} cm^2 s^{-1} at 11°C and 15 psu (core Dec 06), or 1.81×10^{-5} cm^2 s^{-1} at 28°C and 16.6 psu (cores Jul 06–1 and Jul 08-2)] (Sahores and Witherspoon, 1970; Lerman, 1979), c is porewater methane concentration, x is sediment depth, ω is the sediment burial velocity (0.26 cm year^{-1}; Benninger and Martens, 1983) and ΣR is the net reaction rate for methane. The assumptions implicit in this equation are that methane concentrations are at steady state, porosity is constant, molecular diffusion and sedimentation are the dominant transport processes for methane, and vertical concentration gradients are much larger than horizontal gradients.

The net methane reaction rate (production minus consumption) as a function of depth was calculated by inverting Eq. 3 and solving for ΣR. The first and second depth derivatives of the methane concentration were estimated by fitting a smoothing cubic spline function (Alperin *et al.*, 1988) to the methane concentration data. In general, the degree of smoothing was the minimum needed to filter out noise in the methane concentrations that we attribute to sampling and processing artefacts. Positive values of ΣR indicate net methane production, and negative values denote net methane oxidation. Net reaction rates estimated by inverse models are consistent with the concentration data, but they are not unique because the concentration data are not continuous and are to some degree contaminated by error. The greater the scatter in the concentration data, the greater the possibility that the predicted rates may be biased by smoothing. Concordance between the net reaction rates from the inverse model (Fig. 1, column B) and measured concentrations was checked by inputting calculated ΣR values into Eq. 3 and solving by finite difference (solutions are shown as solid curves in Fig. 1, column A).

δ^{13}C-methane profiles were modelled by solving Eq. 3 for ^{12}C-methane (^{12}c) and ^{13}C-methane (^{13}c). Aqueous diffusion coefficients are assumed to be the same for both isotopic species of methane, and the reaction rate terms for ^{12}c ($\Sigma^{12}R$) and ^{13}c ($\Sigma^{13}R$) are represented as:

$$\Sigma^{12}R = MPR\left(\frac{1}{1+F_{MP}}\right) - MOR\left(\frac{\alpha^{12}c}{^{13}c + \alpha^{12}c}\right)$$

$$\Sigma^{13}R = MPR\left(\frac{F_{MP}}{1+F_{MP}}\right) - MOR\left(\frac{^{13}c}{^{13}c + \alpha^{12}c}\right), \qquad (4)$$

where *MPR* and *MOR* are the methane production and oxidation rates, respectively, predicted by the inverse model

(Fig. 1, column B), F_{MP} is the ratio of ^{13}C to ^{12}C in methane produced by methanogenesis (calculated from the δ^{13}C value of methane produced), and α is the kinetic isotope effect for anaerobic methane oxidation. The δ^{13}C of methane produced in these sediments was assumed to be –88‰, based on the fractionation factor for methane production from CO_2 (1.070 at 28°C; Whiticar *et al.*, 1986) and assuming δ^{13}C-ΣCO_2 = –10‰ and that CO_2 is 8‰ enriched in ^{12}C relative to ΣCO_2. To accurately simulate δ^{13}C-methane profiles, methane oxidation rates from the inverse model had to be slightly modified to allow for slow rates in the upper portion of the sulfate reduction zone; methane oxidation rates above the arrows in Fig. 1, Column B (Jul 08-1 and Jul 08-2) represent arbitrary functions that are continuous with methane oxidation rates from the inverse model at 17 cm (Jul 08-1) or 25 cm (Jul 08-2), and attenuate to zero at the sediment–water interface. The kinetic isotope effect (α) was varied so that predicted δ^{13}C -methane profiles best fit the data.

References

Alperin, M.J., and Hoehler, T.M. (2009) Anaerobic methane oxidation by archaea/sulfate-reducing bacteria aggregates: 2. Isotopic constraints. *Am J Sci* **309:** 958–984.

Alperin, M.J., Reeburgh, W.S., and Whiticar, M.J. (1988) Carbon and hydrogen isotope fractionation resulting from anaerobic methane oxidation. *Global Biogeochem Cycles* **2:** 279–288.

Ashelford, K.E., Chuzhanova, N.A., Fry, J.C., Jones, A.J., and Weightman, A.J. (2006) New screening software shows that most recent large 16S rRNA gene clone libraries contain chimeras. *Appl Environ Microbiol* **72:** 5734–5741.

Benninger, L.K., and Martens, C.S. (1983) *Sources and Fates of Sedimentary Organic Matter in the White Oak and Neuse estuaries*. Raleigh, NC, USA: Water Resources Research Institute of the University of North Carolina, UNC-WRRI-83-194.

Berner, R.A. (1980) *Early Diagenesis: A Theoretical Approach*. Princeton, NJ, USA: Princeton University Press.

Blumenberg, M., Seifert, R., Reitner, J., Pape, T., and Michaelis, W. (2004) Membrane lipid patterns typify distinct anaerobic methanotrophic consortia. *Proc Natl Acad Sci USA* **101:** 11111–11116.

Boetius, A., Ravenschlag, K., Schubert, C.J., Rickert, D., Widdel, F., Gieseke, A., *et al.* (2000) A marine microbial consortium apparently mediating anaerobic oxidation of methane. *Nature* **407:** 623–626.

Boone, D.R., Whitman, W.B., and Rouvière, P. (1993) Diversity and taxonomy of methanogens. In *Methanogenesis: Ecology, Physiology, Biochemistry, and Genetics*. Ferry, J.G. (ed). New York, USA: Chapman & Hall, pp. 35–80.

Dekas, A.E., Poretsky, R.S., and Orphan, V.J. (2009) Deep-sea archaea fix and share nitrogen in methane-consuming microbial consortia. *Science* **326:** 422–426.

Eller, G., Känel, L., and Krüger, M. (2005) Cooccurrence of aerobic and anaerobic methane oxidation in the water column of Lake Plußsee. *Appl Environ Microbiol* **71:** 8925–8928.

Elvert, M., and Suess, E. (1999) Anaerobic methane oxidation associated with marine gas hydrates: superlight C-isotopes from saturated and unsaturated C_{20} and C_{25} irregular isoprenoids. *Naturwissenschaften* **86:** 295–300.

Fenchel, R., King, G.M., and Blackburn, T.H. (1998) *Bacterial Biogeochemistry: The Ecophysiology of Mineral Cycling*. San Diego, USA: Academic Press.

Hallam, S.J., Girguis, P.R., Preston, C.M., Richardson, P.M., and DeLong, E.F. (2003) Identification of methyl coenzyme M reductase A (*mcrA*) genes associated with methane-oxidizing archaea. *Appl Environ Microbiol* **69:** 5483–5491.

Hallam, S.J., Putnam, N., Preston, C.M., Detter, J.C., Rokhsar, D., Richardson, P., and DeLong, E.F. (2004) Reverse methanogenesis: testing the hypothesis with environmental genomics. *Science* **305:** 1457–1462.

Harrison, B.K., Zhang, H., Berelson, W., and Orphan, V.J. (2009) Variations in archaeal and bacterial diversity associated with the sulfate-methane transition zone in continental margin sediments (Santa Barbara Basin, California). *Appl Environ Microbiol* **75:** 1487–1499.

Hayes, J.M., Takigiku, R., Ocampo, R., Callot, H.J., and Albrecht, P. (1987) Isotopic compositions and probable origins of organic molecules in the Eocene Messel shale. *Nature* **329:** 48–51.

Hennigan, A.N., and Reeve, J.N. (1994) mRNAs in the methanogenic archaeon *Methanococcus vannielii*: numbers, half-lives and processing. *Mol Microbiol* **11:** 655–670.

Hinrichs, K.-U., Hayes, J.M., Sylva, S.P., Brewer, P.G., and DeLong, E.F. (1999) Methane-consuming archaebacteria in marine sediments. *Nature* **398:** 802–805.

Hoehler, T.M., and Alperin, M.J. (1996) Anaerobic methane oxidation by a methanogen-sulfate reducer consortium: geochemical evidence and biochemical considerations. In *Microbial Growth on C_1 Compounds*. Lidstrom, M.E., and Tabita, F.R. (eds). Boston, USA: Kluwer Academic Publishers, pp. 326–333.

Hoehler, T.M., Alperin, M.J., Albert, D.B., and Martens, C.S. (1994) Field and laboratory studies of methane oxidation in an anoxic marine sediment: evidence for a methanogen-sulfate reducer consortium. *Global Biogeochem Cycles* **8:** 451–463.

Hoehler, T.M., Alperin, M.J., Albert, D.B., and Martens, C.S. (1998) Thermodynamic control on hydrogen concentrations in anoxic sediments. *Geochim Cosmochim Acta* **62:** 1745–1756.

Hoehler, T.M., Alperin, M.J., Albert, D.B., and Martens, C.S. (2001) Apparent minimum free energy requirements for methanogenic archaea and sulfate-reducing bacteria in an anoxic marine sediment. *FEMS Microbiol Ecol* **38:** 33–41.

Holler, T., Wegener, G., Knittel, K., Boetius, A., Brunner, B., Kuypers, M.M.M., and Widdel, F. (2009) Substantial $^{13}C/^{12}C$ and D/H fractionation during anaerobic oxidation of methane by marine consortia enriched *in vitro*. *Environ Microbiol Rep* **1:** 370–376.

House, C.H., Orphan, V.J., Turk, K.A., Thomas, B., Pernthaler, A., Vrentas, J.M., and Joye, S.B. (2009) Extensive carbon isotopic heterogeneity among methane seep microbiota. *Environ Microbiol* **11:** 2207–2215.

Kemp, P.F., Lee, S., and LaRoche, J. (1993) Estimating the growth rate of slowly growing marine bacteria from RNA content. *Appl Environ Microbiol* **59:** 2594–2601.

Kendall, M.M., Wardlaw, G.D., Tang, C.F., Bonin, A.S., Liu, Y., and Valentine, D.L. (2007) Diversity of *Archaea* in marine sediments from Skan Bay, Alaska, including cultivated methanogens, and description of *Methanogenium boonei* sp. nov. *Appl Environ Microbiol* **73:** 407–414.

Knittel, K., and Boetius, A. (2009) Anaerobic oxidation of methane: progress with an unknown process. *Annu Rev Microbiol* **63:** 311–334.

Knittel, K., Lösekann, T., Boetius, A., Kort, R., and Amann, R. (2005) Diversity and distribution of methanotrophic archaea at cold seeps. *Appl Environ Microbiol* **71:** 467–479.

Krüger, M., Meyerdierks, A., Glöckner, F.-O., Amann, R., Widdel, F., Kube, M., *et al.* (2003) A conspicuous nickel protein in microbial mats that oxidize methane anaerobically. *Nature* **426:** 878–881.

Lanoil, B.D., Sassen, R., La Duc, M.T., Sweet, S.T., and Nealson, K.H. (2001) *Bacteria* and *Archaea* physically associated with Gulf of Mexico gas hydrates. *Appl Environ Microbiol* **67:** 5143–5153.

Lerman, A. (1979) *Geochemical Processes: Water and Sediment Environments*. Hoboken, NJ, USA: John Wiley and Sons.

Lloyd, K.G., MacGregor, B.J., and Teske, A. (2010) Quantitative PCR methods for RNA and DNA in marine sediments: maximizing yield while overcoming inhibition. *FEMS Microbiol Ecol* **72:** 143–151.

Londry, K.L., Dawson, K.G., Grover, H.D., Summons, R.E., and Bradley, A.S. (2008) Stable carbon isotope fractionation between substrates and products of *Methanosarcina barkeri*. *Org Geochem* **39:** 608–621.

Lösekann, T., Knittel, K., Nadalig, T., Fuchs, B., Niemann, H., Boetius, A., and Amann, R. (2007) Diversity and abundance of aerobic and anaerobic methane oxidizers at the Haakon Mosby mud volcano, Barents Sea. *Appl Environ Microbiol* **73:** 3348–3362.

Lovley, D.R., Dwyer, D.F., and Klug, M.J. (1982) Kinetic analysis of competition between sulfate reducers and methanogens for hydrogen in sediments. *Appl Environ Microbiol* **43:** 1373–1379.

Loy, A., Duller, S., Baranyi, C., Mußmann, M., Ott, J., Sharon, I., *et al.* (2009) Reverse dissimilatory sulfite reductase as phylogenetic marker for a subgroup of sulfur-oxidizing prokaryotes. *Environ Microbiol* **11:** 289–299.

Ludwig, W., Strunk, O., Westram, R., Lothar, R., Meier, H., Yadhukumar, *et al.* (2004) ARB: A software environment for sequence data. *Nuc Acids Res* **32:** 1363–1371.

Luton, P.E., Wayne, J.M., Sharp, R.J., and Riley, P.W. (2002) The *mcrA* gene as an alternative to 16S rRNA in the phylogenetic analysis of methanogen populations in landfill. *Microbiology* **148:** 3521–3530.

Martens, C.S., Albert, D.B., and Alperin, M.J. (1998) Biogeochemical processes controlling methane in gassy coastal sediments – Part I. A model coupling organic matter flux to gas production, oxidation and transport. *Cont Shelf Res* **18:** 1741–1770.

Meyerdierks, A., Kube, M., Kostadinov, I., Teeling, H., Glöckner, F.O., Reinhardt, R., and Amann, R. (2010) Metagenome and mRNA expression analyses of anaerobic methanotrophic archaea of the ANME-1 group. *Environ Microbiol* **12:** 422–439.

Michaelis, W., Seifert, R., Nauhaus, K., Treude, T., Thiel, V., Blumenberg, M., *et al.* (2002) Microbial reefs in the Black Sea fueled by anaerobic oxidation of methane. *Science* **297:** 1013–1015.

Mills, H.J., Hodges, C., Wilson, K., MacDonald, I.R., and Sobecky, P.A. (2003) Microbial diversity in sediments associated with surface-breaching gas hydrate mounds in the Gulf of Mexico. *FEMS Microbiol Ecol* **46:** 39–52.

Munson, M.A., Nedwell, D.B., and Embley, T.M. (1997) Phylogenetic diversity of *Archaea* in sediment samples from a coastal salt marsh. *Appl Environ Microbiol* **63:** 4729–4733.

Murray, P., and Zinder, S.H. (1984) Nitrogen fixation by a methanogenic archaebacterium. *Nature* **312:** 284–286.

Neretin, L.N., Schippers, A., Pernthaler, A., Hamann, K., Amann, R., and Jørgensen, B.B. (2003) Quantification of dissimilatory (bi) sulphite reductase gene expression in *Desulfobacterium autotrophicum* using real-time RT-PCR. *Environ Microbiol* **5:** 660–671.

Niemann, H., Elvert, M., Hovland, M., Orcutt, B., Judd, A., Suck, I., *et al.* (2005) Methane emission and consumption at a North Sea gas seep (Tommeliten area). *Biogeosciences* **2:** 335–351.

Niemann, H., Duarte, J., Hensen, C., Omoregie, E., Magalhães, V.H., Elvert, M., *et al.* (2006) Microbial methane turnover at mud volcanoes of the Gulf of Cadiz. *Geochim Cosmochim Acta* **70:** 5336–5355.

Omoregie, E.O., Mastalerz, V., de Lange, G.J., Straub, K.L., Kappler, A., Røy, H., *et al.* (2008) Biogeochemistry and community composition of iron- and sulfur-precipitating microbial mats at the Chefren Mud Volcano (Nile Deep Sea Fan, Easter Mediterranean). *Appl Environ Microbiol* **74:** 3198–3215.

Omoregie, E.O., Niemann, H., Mastalerz, V., de Lange, G.J., Stadnitskaia, A., Foucher, J.-P., and Boetius, A. (2009) Microbial methane oxidation and sulfate reduction at cold seeps of the deep Eastern Mediterranean Sea. *Mar Geol* **261:** 114–127.

Orcutt, B., Boetius, A., Elvert, M., Samarkin, V., and Joye, S.B. (2005) Molecular biogeochemistry of sulfate reduction, methanogenesis and the anaerobic oxidation of methane at Gulf of Mexico cold seeps. *Geochim Cosmochim Acta* **69:** 4267–4281.

Orcutt, B., Samarkin, V., Boetius, A., and Joye, S. (2008) On the relationship between methane production and oxidation by anaerobic methanotrophic communities from cold seeps of the Gulf of Mexico. *Environ Microbiol* **10:** 1108–1117.

Orphan, V.J., House, C.H., Hinrichs, K.-U., McKeegan, K.D., and DeLong, E.F. (2001) Methane-consuming archaea revealed by directly coupled isotopic and phylogenetic analysis. *Science* **293:** 484–487.

Orphan, V.J., House, C.H., Hinrichs, K.-U., McKeegan, K.D., and DeLong, E.F. (2002) Multiple archaeal groups mediate methane oxidation in anoxic cold seep sediments. *Proc Natl Acad Sci USA* **99:** 7663–7668.

Parkes, R.J., Cragg, B.A., Banning, N., Brock, F., Webster, G., Fry, J.C., *et al.* (2007) Biogeochemistry and biodiversity of methane cycling in subsurface marine sediments (Skagerrak, Denmark). *Environ Microbiol* **9:** 1146–1161.

Pernthaler, A., Dekas, A.E., Brown, T., Goffredi, S.K., Embaye, T., and Orphan, V.J. (2008) Diverse syntrophic partnerships from deep-sea methane vents revealed by direct cell capture and metagenomics. *Proc Natl Acad Sci USA* **105:** 7052–7057.

Pimenov, N.V., Rusanov, I.I., Poglazova, M.N., Mityushina, L.L., Sorokin, D.Y., Khmelenina, V.N., and Trotsenko, Y.A. (1997) Bacterial mats on coral-like structures at methane seeps in the Black Sea. *Microbiology* **66:** 354–360.

Polz, M.F., and Cavanaugh, C.M. (1997) A simple method for quantification of uncultured microorganisms in the environment based on *in vitro* transcription of 16S rRNA. *Appl Environ Microbiol* **63:** 1028–1033.

Pruesse, E., Quast, C., Knittel, K., Fuchs, B.M., Ludwig, W., Peplies, J., and Glöckner, F.O. (2007) SILVA: a comprehensive online resource for quality checked and aligned ribosomal RNA sequence data compatible with ARB. *Nucleic Acids Res* **35:** 7188–7196.

Reeburgh, W.S. (2007) Oceanic methane biogeochemistry. *Chem Rev* **107:** 486–513.

Sahores, J.J., and Witherspoon, P.A. (1970) *Diffusion of Light Paraffin Hydrocarbons in Water from 2°C to 80°C*. In *Advances in Organic Geochemistry*. Spears, G.C. (ed.). New York, USA: Pergammon, pp. 219–230.

Santegoeds, C.M., Damgaard, L.R., Hesselink, G., Zopfi, J., Lens, P., Muyzer, G., and de Beer, D. (1999) Distribution of sulfate-reducing and methanogenic bacteria in anaerobic aggregates determined by microsensor and molecular analyses. *Appl Environ Microbiol* **65:** 4618–4629.

Scheller, S., Goenrich, M., Boecher, R., Thauer, R.K., and Jaun, B. (2010) The key nickel enzyme of methanogenesis catalyses the anaerobic oxidation of methane. *Nature* **465:** 606–609.

Schloss, P.D., and Handelsman, J. (2005) Introducing DOTUR, a computer program for defining operational taxonomic units and estimating species richness. *Appl Environ Microbiol* **71:** 1501–1506.

Schloss, P.D., and Handelsman, J. (2006) Introducing SONS, a tool for operational taxonomic unit-based comparisons of microbial community memberships and structures. *Appl Environ Microbiol* **72:** 6773–6779.

Schreiber, L., Holler, T., Knittel, K., Meyerdierks, A., and Amann, R. (2010) Identification of the dominant sulfate-reducing bacterial partner of the anaerobic methanotrophs of the ANME-2 clade. *Environ Microbiol* **12:** 2327–2340.

Seifert, R., Nauhaus, K., Blumenberg, M., Krüger, M., and Michaelis, W. (2006) Methane dynamics in a microbial

community of the Black Sea traced by stable carbon isotopes *in vitro. Org Geochem* **37:** 1411–1419.

Senior, E., Lindström, E.B., Banat, I.M., and Nedwell, D.B. (1982) Sulfate reduction and methanogenesis in the sediment of a saltmarsh on the east coast of the United Kingdom. *Appl Environ Microbiol* **43:** 987–996.

Siegert, M., Cichocka, D., Herrmann, S., Gründger, F., Feisthauer, S., Richnow, H.-H., *et al.* (2010) Accelerated methanogenesis from aliphatic and aromatic hydrocarbons under iron- and sulfate-reducing conditions. *FEMS Microbiol Lett* **315:** 6–16.

Srivastava, A.K., and Schlessinger, D. (1990) Mechanism and regulation of bacterial ribosomal RNA processing. *Annu Rev Microbiol* **44:** 105–129.

Swofford, D.L. (2000) *PAUP*. Phylogenetic Analysis Using Parsimony (and Other Methods), Version 4.0b10*. Sunderland, MA, USA: Sinauer Associates.

Thomsen, T.R., Finster, K., and Ramsing, N.B. (2001) Biogeochemical and molecular signatures of anaerobic methane oxidation in a marine sediment. *Appl Environ Microbiol* **67:** 1646–1656.

Treude, T., Kruger, M., Boetius, A., and Jorgensen, B.B. (2005) Environmental control on anaerobic oxidation of methane in the gassy sediments of Eckernforde Bay (German Baltic). *Limnol Oceanogr* **50:** 1771–1786.

Treude, T., Orphan, V.J., Knittel, K., Gieseke, A., House, C.H., and Boetius, A. (2007) Consumption of methane and CO_2 by methanotrophic microbial mats from gas seeps of the anoxic Black Sea. *Appl Environ Microbiol* **73:** 2271–2283.

Ullman, W.J., and Aller, R.C. (1982) Diffusion coefficients in nearshore marine sediments. *Limnol Oceanogr* **27:** 552–556.

Whiticar, M.J., Faber, E., and Schoell, M. (1986) Biogenic methane formation in marine and freshwater environments: CO_2 reduction vs. acetate fermentation – isotope evidence. *Geochim Cosmochim Acta* **50:** 693–709.

Willerslev, E., Hansen, A.J., Rønn, R., Brand, T.B., Barnes, I., Wiuf, C., *et al.* (2004) Long-term persistence of bacterial DNA. *Curr Biol* **14:** R9–R10.

Yamamoto, S., Alcauskas, J.B., and Crozier, T.E. (1976) Solubility of methane in distilled water and seawater. *J Chem Engin Data* **21:** 78–80.

Zehnder, A.J.B., and Brock, T.D. (1979) Methane formation and methane oxidation by methanogenic bacteria. *J Bacteriol* **137:** 420–432.

Supporting information

Additional Supporting Information may be found in the online version of this article:

Table S1. RNA extraction details and primer combinations used for 16S rRNA, *mcrA* mRNA and *dsrAB* mRNA clone libraries for all the cores.

Table S2. Primers used for reverse transcription and amplification for cDNA clone libraries.

Fig. S1. Neighbour-joining tree of methanogen-related archaeal 16S rRNA transcript sequences, with distance- or parsimony-based bootstrap support ($> 60\%$) from 1000 repetitions listed at the nodes, respectively, excluding the poorly aligned helix 6. Numbers of clones represented by each 97% OTU group within each core and depth are shown in parentheses. Cores are named A for Jul 05-1, B for Jul 05-2, E for Dec 06 and G for Jul 08-2. Clones from the AOM zone are in red, clones from the methanogenesis zone are in blue and tree was rooted with *Methanocaldococcus jannaschii*. Scale bar represents 10% distance.

Fig. S2. Neighbour-joining trees of amino acid translations of *dsrAB* mRNA cDNA following the groupings of Leloup and colleagues (2007) (14) and Zverlov and colleagues (2005) (15), with distance- and then parsimony-based bootstrap support ($> 60\%$) from 1000 repetitions listed at the nodes. Numbers of clones represented by each 97% OTU group (determined from nucleic acids) are shown in parentheses. Clones from the AOM zone are in red, clones from the methanogenesis zone are in blue, with naming conventions as for Fig. S1.

Fig. S3. Percentage of positive RT-PCR amplification attempts for *mcrA* mRNA (using only general *mcrA* primers, excluding the ANME-1 mcrf/r which are specific for ANME-1) and *dsrAB* mRNA within the AOM (red) and the methanogenic (blue) zones for cores Jul 05-1, Jul 05-2, Dec 06 and Jul 08-2. Values are significantly different between AOM and methanogenesis zones ($P > 99\%$ for *mcrA*, $P > 98\%$ for *dsrA*) with a two-tailed chi-squared test, and the numbers written on the bars are the total numbers of amplification attempts. Only amplification attempts with primers and RT-PCR conditions that had previously been shown to result in a positive amplification were included.

Fig. S4. Map of the coast of North Carolina and the White Oak River, near Beaufort, North Carolina. Inset shows the location of station H as the river opens up into brackish estuarine sediments. Map made using the free Online Map Creation tool at http://www.aquarius.ifm-geomar.de.